Research article

Nicolò Accanto, Pablo M. de Roque, Marcial Galvan-Sosa, Ion M. Hancu and Niek F. van Hulst*

Selective excitation of individual nanoantennas by pure spectral phase control in the ultrafast coherent regime

https://doi.org/10.1515/nanoph-2020-0406
Received July 20, 2020; accepted August 5, 2020; published online September 7, 2020

Abstract: Coherent control is an ingenious tactic to steer a system to a desired optimal state by tailoring the phase of an incident ultrashort laser pulse. A relevant process is the two-photon–induced photoluminescence (TPPL) of nanoantennas, as it constitutes a convenient route to map plasmonic fields, and has important applications in biological imaging and sensing. Unfortunately, coherent control of metallic nanoantennas is impeded by their ultrafast femtosecond dephasing times so far limiting control to polarization and spectral optimization. Here, we report that phase control of the TPPL in resonant gold nanoantennas is possible. We show that, by compressing pulses shorter than the localized surface plasmon dephasing time (<20 fs), a very fast coherent regime develops, in which the two-photon excitation is sensitive to the phase of the electric field and can therefore be controlled. Instead, any phase control is gone when using longer pulses. Finally, we demonstrate pure phase control by resorting to a highly sensitive closed-loop strategy, which exploits the phase differences in the ultrafast coherent response of different nanoantennas, to selectively excite a chosen antenna. These results underline the direct and intimate relation between TPPL and coherence in gold nanoantennas, which makes them interesting systems for nanoscale nonlinear coherent control.

Keywords: closed-loop control; coherent control; hot spot; nanoantenna; spectral phase control; ultrafast.

1 Introduction

In the field of optics, coherent control refers to the capability of precisely tailored laser fields to actively manipulate the outcome of certain light–matter interactions by exploiting the coherent properties of the system under study. One common experimental implementation of coherent control makes use of broadband phase-controlled laser pulses to generate interference phenomena [1–6]. By inducing constructive interference between the pathways that connect the initial state to the desired final state and destructive interference among those leading to unwanted final states, the laser pulse actively steers the investigated system towards the desired target. However, because interference is strictly related to phase, this approach to coherent control is only applicable to systems that retain the phase information for a sufficiently long time, i.e. for a time longer than the pulse duration [3, 4, 6]. In the coherent control formalism, the characteristic time after which the system loses its phase memory is called dephasing or coherence time and is indicated with T_2. The condition for coherent control to be effective is thus that $T_2 > \delta$, where δ represents the pulse duration. Systems with T_2 shorter than the pulse duration are elusive to coherent control.

Optical nanoantennas are metallic nanostructures that support localized surface plasmon resonances (LSPRs) in the optical or near-infrared spectral region. Light couples

Present address: Pablo M. de Roque, KPMG Lighthouse – Data Analytics & AI, 08908 L'Hospitalet de Llobregat, Barcelona, Spain; and **Ion M. Hancu,** Gauss & Neumann, Search Engine Marketing Technology.

***Corresponding author: Niek F. van Hulst**, ICFO—Institut de Ciences Fotoniques, The Barcelona Institute of Science & Technology, 08860 Castelldefels, Barcelona, Spain; and ICREA—Institució Catalana de Recerca i Estudis Avançats, 08010 Barcelona, Spain, E-mail: Niek.vanHulst@icfo.eu. https://orcid.org/0000-0003-4630-1776

Nicolò Accanto, ICFO—Institut de Ciences Fotoniques, The Barcelona Institute of Science & Technology, 08860 Castelldefels, Barcelona, Spain; and Institut de la Vision, Sorbonne Université, Inserm S968, CNRS UMR7210, 17 Rue Moreau, 75012 Paris, France, E-mail: nicolo.accanto@inserm.fr. https://orcid.org/0000-0003-2491-7190

Pablo M. de Roque and Ion M. Hancu, ICFO—Institut de Ciences Fotoniques, The Barcelona Institute of Science & Technology, 08860 Castelldefels, Barcelona, Spain, E-mail: pablom.roque@gmail.com (P. M. de Roque), im.hancu@gmail.com (I. M. Hancu). https://orcid.org/0000-0002-0751-9126 (P. M. de Roque)

Marcial Galvan-Sosa, Neurochemistry and Neuroimaging Laboratory, University of La Laguna, Tenerife, Spain, E-mail: igalvans@ull.es

to the nanoantennas driving a LSPR confined to the nanoantenna surface, providing control of the near fields at subwavelength spatial scales [7]. Optical nanoantennas are used to direct light emission [8–10], to change excitation and emission rates in molecules [11–13], to improve nonlinear optical effects [14] and as active elements for sensing [15, 16]. Two-photon–induced photoluminescence (TPPL) microscopy, in which an ultrashort laser pulse induces two-photon excitation (TPE), is one of the most commonly used techniques to map surface plasmons in optical nanoantennas [17–19]. In recent years, the TPPL from gold nanoantennas emerged as a promising contrast mechanism for biological imaging and even for cancer therapy [20–22]. The perspective of coherent control strategies to manipulate TPPL in gold nanoantennas by tuning the phase of the laser pulse is attractive for optimal contrast control.

Stockman et al. [23] and Stockman [24] first linked the field of coherent control to the study of optical nanoantennas with the objective of simultaneously achieving nanometre and femtosecond control of optical fields. Experimental demonstrations of such control principle include: the phase and polarization manipulation of nanooptical fields in the incoherent regime [25, 26]; the simultaneous high space and time resolution imaging of surface plasmon dynamics in the coherent and incoherent regimes [27–33]; and the phase-dependent control of the propagation of LSPRs through nanoparticle arrays caused by different amounts of dispersion acquired in different propagation directions [34, 35].

The TPPL in gold nanoantennas was studied by Biagioni et al. [18] as a function of increasing chirp applied to an ultrashort pulse. The observed lack of change in the TPPL for pulses shorter than 100 fs was interpreted as stemming from a two-step single photon absorption involving an intermediate state, as also shown in other works [36, 37]. In contrast, phase dependence of the TPPL on a rough gold film was reported [38], and such dependence was used to deduce the LSPRs of different gold nanoantennas [39]. These early works point towards the necessity of a unique model to clear out the origin of the phase dependence of the TPPL in gold nanoantennas and to find under which conditions coherent phase control in these systems can be made to use.

Here, we show that the intrinsic nature of the TPE in gold nanoantennas, in which an intermediate state (the LSPR) mediates the process, leads to a very fast initial coherent regime. This regime is only accessible by ultrashort laser pulses, shorter than the coherence time T_2 (<50 fs), for which the TPE is sensitive to the spectral phase of the electric field. We then demonstrate that phase-only coherent control is capable to manipulate the TPE in different nanoantennas and obtain contrast in the emitted TPPL. To achieve this, we used a newly developed closed-loop phase control scheme with single-molecule sensitivity [40] that adapts to the subtle differences in the coherent response of different nanoantennas with detuned LSPRs to selectively excite them.

2 The initial coherent regime

In order to unveil the coherent response of gold nanoantennas, we first investigated the ultrafast dynamics of the TPE by varying the excitation pulse duration in the range of 15 fs–1 ps and detecting the TPPL with a high-resolution confocal microscope (see Methods). As sketched in Figure 1a, we used a pulse shaper to actively control the spectral phase $\varphi(\omega)$ of the laser field, which allowed us to change the pulse duration by applying different amounts of linear chirp.

The time duration dependence of the TPPL from a single resonant 90 nm gold nanorod antenna is plotted in Figure 1b, together with that of the second harmonic (SH) produced by a single nonresonant barium–titanate ($BaTiO_3$) nanoparticle that provides the reference for a pure TPE process. As expected from theory [41], the SH intensity scales as the inverse of the pulse duration δ, being maximal for the shortest laser pulse. In contrast, the TPPL from the gold nanoantenna presents a very different behaviour, and three regimes can be identified: (i) for $\delta \lesssim 50$ fs, the TPPL increases as the pulse duration decreases; (ii) for $100 \lesssim \delta \lesssim 300$ fs, the TPPL is almost constant; (iii) for $\delta \gtrsim 300$ fs, the dependence on the inverse of δ is recovered. Regimes (ii) and (iii) were already studied in the study by Biagioni et al. [18] and are consistent with the established model in which the TPE process in gold involves two successive single-photon absorptions, mediated by a real transition with lifetime T_1 in the few hundreds to thousands femtosecond range [18, 19, 32, 37]. For nanoantennas resonant in the spectral region of the excitation spectrum, the LSPR acts as the intermediate state, enhancing the TPE process [32, 37]. In this model, a second photon can induce TPE if it impinges on the system before the intermediate state population excited by a first photon has decayed, which explains the observed TPPL dependence in regimes (ii) and (iii). This behaviour can be described mathematically as follows [18]:

$$\mathrm{TPE}_{\delta>100} \propto \int E_\delta(t)dt \int E_\delta(t-t_1)e^{-t_1/T_{LF}}dt_1 \qquad (1)$$

where $E_\delta(t)$ represents the time-varying electric field as a function of the pulse duration δ. A fit of the experimental

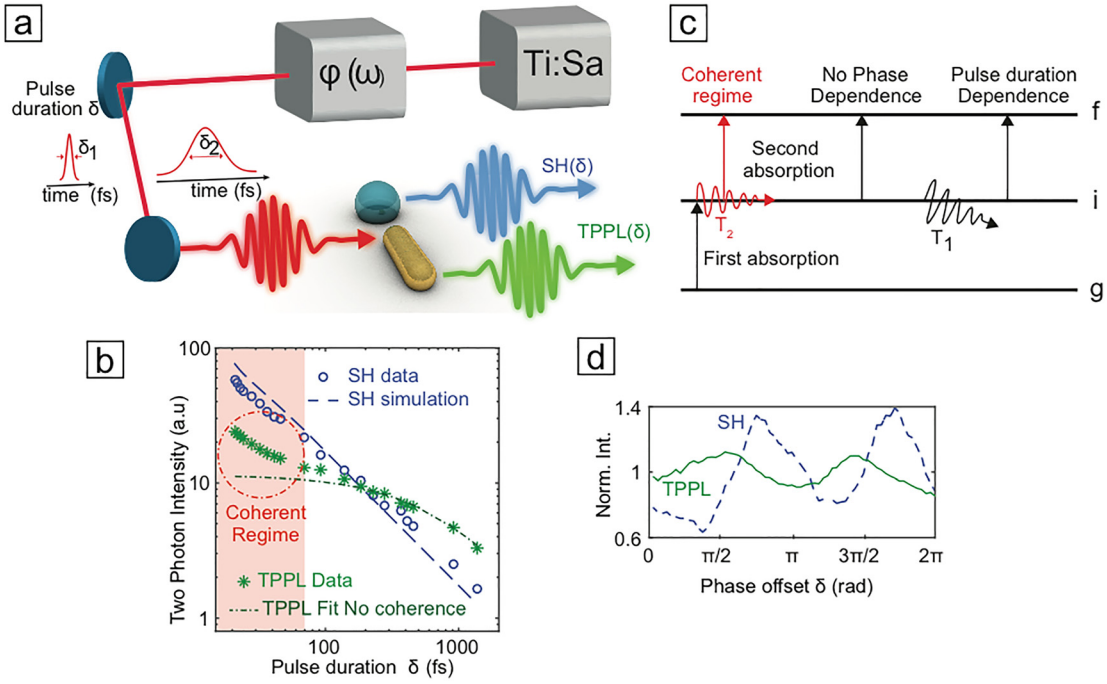

Figure 1: TPPL as a function of the pulse duration.
(a) Schematic of the experiment: a pulse shaper changes the time duration of a laser pulse in the range of 15 fs–1 ps. The TPPL from a resonant nanoantenna and the SH from a nonresonant $BaTiO_3$ are detected as a function of the pulse duration. (b) Experimental dependence of the SH (blue circles) and the TPPL from a resonant 90-nm long gold nanoantenna (green stars) on the pulse length δ. The blue dashed curve is the predicted behaviour of the SH, which agrees well with the experiment. The dark green dot-dashed curve corresponds to a fit to the TPPL for $\delta > 100$ fs using Eq. (1) from which we infer a lifetime of the intermediate state $T_1 \cong 350 \pm 50$ fs. For pulses shorter than ~50 fs, a coherent regime develops. (c) Sketch of the three different regimes involved in TPE as a function of the pulse length. (d) Effect of a spectral phase scan on the TPPL from a resonant gold nanoantenna (green curve) and the SH from a $BaTiO_3$ nanoparticle (blue curve). Note that the modulation depth is substantially reduced for the TPPL response. TPPL, two-photon–induced photoluminescence; TPE, two-photon excitation; SH, second harmonic.

TPPL data in Figure 1b using Eq. (1) produces the dark green dot-dashed curve, which well reproduces the experimental points for $\delta \gtrsim 100$ fs, yielding a lifetime $T_1 = 350 \pm 50$ fs, a bit shorter than the value of 650 fs reported by Biagioni et al. [19]. The lifetime should be compared to typical relaxation rates of the hot electron gas in noble metals [42, 43]. The TPE in gold can be understood on the basis of the gold band structure as follows [18, 36]: the first photon induces an intraband transition that excites an electron to the *sp* conduction band above the Fermi level, leaving a hole in the *sp* conduction band below the Fermi level. The second photon successively induces an interband transition, exciting an electron from the *d* band to the *sp* band, which can recombine with the previously created *sp* hole. The first photon in this picture creates a nonequilibrium situation (hot electrons) that has to decay to the thermal equilibrium. Typical internal thermalization times of the hot electron gas in noble metals were determined to be in the range of 350 fs–3 ps [42–44]. Biagioni et al. [19] reported on crystalline gold gap-antennas, while we study amorphous gold nanorod antennas, which will explain our shorter value of T_1.

Equation (1), however, completely fails to describe the behaviour of the TPPL for $\delta \lesssim 50$ fs, exactly where our experiment is most sensitive. Equation (1) was derived under the explicit assumption that coherent (and thus phase) effects can be neglected for sufficiently long laser pulses [18]. The dephasing time T_2 associated with LSPRs is in the order $T_2 \sim 20$ fs and thus within the time resolution achievable with our experiment [27–32, 45]. We therefore attribute the deviation of the experimental points for $\delta \lesssim 50$ fs from the prediction of Eq. (1) to the development of a coherent regime in which the interaction of the two successive single photons with the nanoantenna depends on the relative phase of the two photons. In this regime, Eq. (1) needs to be modified to account for phase effects.

The phase dependence of resonance-mediated TPE processes was studied for the case of very narrow absorption lines in atoms [46] and for relatively broader absorptions in rare Earth systems [47], in both cases under the

assumption of pulse durations much shorter than the dephasing time of the intermediate state. None of those cases is therefore directly applicable here. For $\delta \lesssim 50$ fs and not considering other plasmonic resonances at the two-photon energy, the TPE can be written as follows [47]:

$$\mathrm{TPE}_{\delta<50} \propto \int d\omega_f \left| \int d\omega_i \, A(\omega_i) E_A(\omega_f - \omega_i) E_A(\omega_i) \right|^2 \quad (2)$$

where $A(\omega)$ is a real function corresponding to the LSPR that mediates the excitation, and the term $E_A(\omega)$ is the complex electric field at the nanoantenna, consisting of an amplitude and a spectral phase component $\varphi(\omega)$. Following the formalism we used in a recent work [48] and neglecting the small contribution from the intrinsic phase response of the nanoantenna, $E_A(\omega)$ can be written as $E_A(\omega) = E(\omega)A(\omega)$, where $E(\omega)$ is the complex laser field. In this limit, the phase dependence in the TPE is recovered. Moreover, considering that $A(\omega)$ is a real function, the dependence on the spectral phase predicted by Eq. (2) is similar to that of the SH from a broadband pulse (see, for example, the study by Lozovoy et al. [41]). Indeed, for very short pulse durations, the TPPL in Figure 1b almost recovers a $\sim\delta^{-1}$ dependence, similar to the SH curve, which strongly supports our interpretation.

To verify the phase dependence of the TPPL, we performed phase scans on a resonant gold nanoantenna (detecting the TPPL) and compared it directly to the SH trace measured from a $BaTiO_3$ nanoparticle. Specifically, we carried out a multiphoton intrapulse interference phase scan (MIIPS), ramping a sinusoidal phase modulation through the laser spectrum [49, 50]. The effect of the spectral phase scanning on TPPL and SH is shown in Figure 1d. Clearly, the two traces show an oscillatory character, with maxima and minima located at different positions. The TPPL does show phase response, yet the total modulation depth is higher in the case of the SH nanoparticle. This difference can be explained based on the three-level model discussed above. As the pulse in the MIIPS is in the range of 20–100 fs, the green curve in Figure 1d is probing a regime in which the intermediate state dynamics starts to kick in, decreasing the achievable modulation depth. In fact, MIIPSs on gold nanoantennas using pulses longer than 100 fs do not show any modulation at all. Our current findings also explain earlier MIIPSs on gold nanoantennas, detecting TPPL to obtain information on their LSPRs [39]. In those scans, as the phase was changed, the time duration of the pulse also varied; as a result, the TPPL showed dependence on the MIIPS, yet mixing phase dependence with time-dependent signature of the intermediate state [39].

From the pulse length dependence, we conclude that, the TPE process in gold nanoantennas is governed by two different timescales: the dephasing time of the surface plasmons T_2 and the lifetime of the intermediate state T_1 (see Figure 1c). For laser pulses with durations comparable with T_2, the TPE is sensitive to the spectral phase of the electric field and pure coherent control becomes possible [51].

3 Closed-loop coherent control of pairs of nanoantennas

We then demonstrated such coherent control by resorting to a closed-loop optimization strategy, in which a deterministic algorithm [40, 52] adjusts the phase of the laser field in order to maximize the targeted signal. From Eq. (2), one can verify that the TPE in a gold nanoantenna is maximized by the shortest possible pulse (the Fourier limited pulse) [47]. Performing a blind maximization of the TPPL on a single nanoantenna would therefore produce Fourier limited pulses, which is a trivial control experiment. To test the control efficiency on the ultrafast TPE, we simultaneously excited two nanorod antennas of different but precisely defined lengths, characterized by different LSPRs and $A(\omega)$ terms, and used the ratio of their emitted TPPL as the feedback variable for the maximization. The concept of the experiment is sketched in Figure 2a (detail in Methods).

First, we acquired a two-dimensional TPPL image of an array of nanoantennas in the sample (Figure 2b). The nanoantennas were fabricated in lines of paired antennas. The length of the lower nanoantennas in the pair was kept constant at 90 nm, whereas the upper nanoantenna length was swept from 100–190 nm. The TPPL image in Figure 2b was taken using a Fourier limited excitation pulse. Based on Figure 2b, nanoantennas of length in the range of 90–120 nm produced the highest signals and therefore were resonant with the excitation laser. Moreover, since the spectral position of LSPRs depends on the length of the nanoantennas (for a fixed width), from Figure 2b we expect 90 nm (120 nm) – long antennas to be resonant with the blue (red) side of the laser spectrum (simulations shown in Figure 3 confirm this). In order to obtain the best control, understood as the highest obtainable contrast compatible with our laser spectrum, we implemented the closed-loop optimization on a pair of 90–120 nm nanoantenna. The feedback variable for the search algorithm was the quotient $A_{120\mathrm{nm}}/A_{90\mathrm{nm}}$, which represents the ratio between the TPPL from the 120 nm and the 90 nm nanoantenna in the pair.

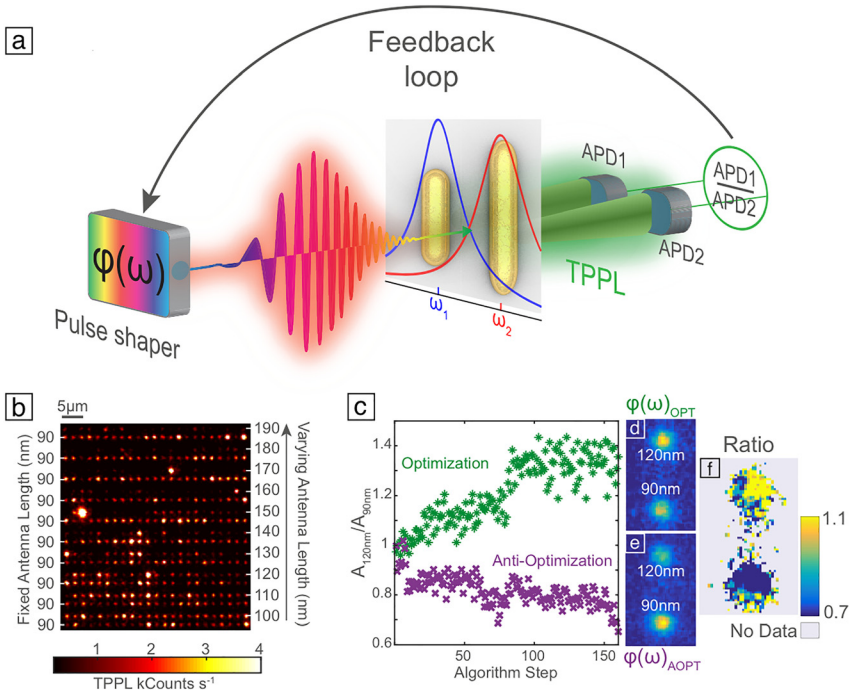

Figure 2: Closed-loop control experiment. (a) The pulse shaper controls the spectral phase of the laser pulse, which simultaneously excites two resonant nanoantennas, characterized by detuned plasmon resonances ω_1 and ω_2, inducing TPE. The TPPL generated by the nanoantennas is sent to two different single-photon avalanche photodiodes (APD1 and APD2), and the ratio between the two signals (APD1/APD2) is maximized in a feedback loop optimization. The search algorithm determines the spectral phase that enhances the ratio of the two-photon excitation in the nanoantennas. (b) Two-photon–induced photoluminescence image of an array of nanoantennas showing the arrangement of the nanoantennas in the sample: fixed length of 90 nm alternating with increasing length (100–190 nm) from bottom to top and the same length for each row. Note that the nanoantennas giving the highest signal (90–120 nm) are the ones that are resonant with the laser spectrum. (c) Plot of the A_{120nm}/A_{90nm} ratio as a function of the algorithm step for both the optimization and antioptimization case. (d, e) TPPL images of the two nanoantennas taken with the optimization ($\varphi(\omega)_{OPT}$) and antioptimization phase ($\varphi(\omega)_{AOPT}$), respectively. Note that the maximum of the two-photon–induced photoluminescence switches from the 120 nm to the 90 nm antenna. (f) Ratio between images d and e emphasizing the contrast between the two nanoantennas. TPPL, two-photon–induced photoluminescence; TPE, two-photon excitation.

We performed two distinct coherent control experiments: in the first one (called optimization experiment), the algorithm maximized A_{120nm}/A_{90nm} and in the second one (antioptimization) instead, minimized it. The results of the two experiments are plotted in Figure 2c as a function of the algorithm step. Experimental data are normalized such that the initial A_{120nm}/A_{90nm} value (corresponding to the Fourier limited pulses) is one. As Figure 2c clearly shows, in the optimization and the antioptimization experiment, the ratio A_{120nm}/A_{90nm} changed, with a final contrast being approximately 2. The spectral phases obtained at the end of the coherent control experiment are called $\varphi(\omega)_{OPT}$ and $\varphi(\omega)_{AOPT}$ and correspond to the optimization and antioptimization case, respectively. Imaging the two nanoantennas using these phases produced the images shown in Figure 2d and e from which one can see that the TPPL maximum switched from one nanoantenna to the other. To make the contrast even more apparent, in Figure 2f, we plot the ratio between Figure 2d and e. To produce this image (and equivalently Figure 3a), we discarded any pixel in which the signal was lower than 200 counts s–1, as they correspond to areas in which no nanoantenna was present, and the signal was only generated by random dark counts in the avalanche photodiodes (APDs).

These results prove that closed-loop coherent control of the TPE in single nanoantennas is possible. To emphasize the role of coherence, we wish to stress that the algorithm acted purely on the spectral phase of the laser pulse, while the laser intensities over the full spectrum were kept constant. Therefore, during an optimization, the laser always resonantly excited the LSPRs of each nanoantennas in the same way, keeping the populations of the intermediate states constant. The control derives from an interference process occurring purely among photons at the energy of the final state, which results in the modulation of the final state populations. This is in contrast to experiments in which the delay between two pulses is varied, as, for instance, in the studies by Kubo et al. [27], Sun et al. [28] and Nishiyama et al. [32]. Scanning the delay between two pulses effectively changes the excitation spectrum and therefore modulates the population of the intermediate state, which is reflected in the population of the final state. At the same time, the results shown here could not be obtained by using longer pulses [25, 26], as these would not interact coherently with the nanoantennas.

We next checked the robustness of the found solutions for nanoantennas of the same type. The upper image in Figure 3a is a contrast image (obtained with the same

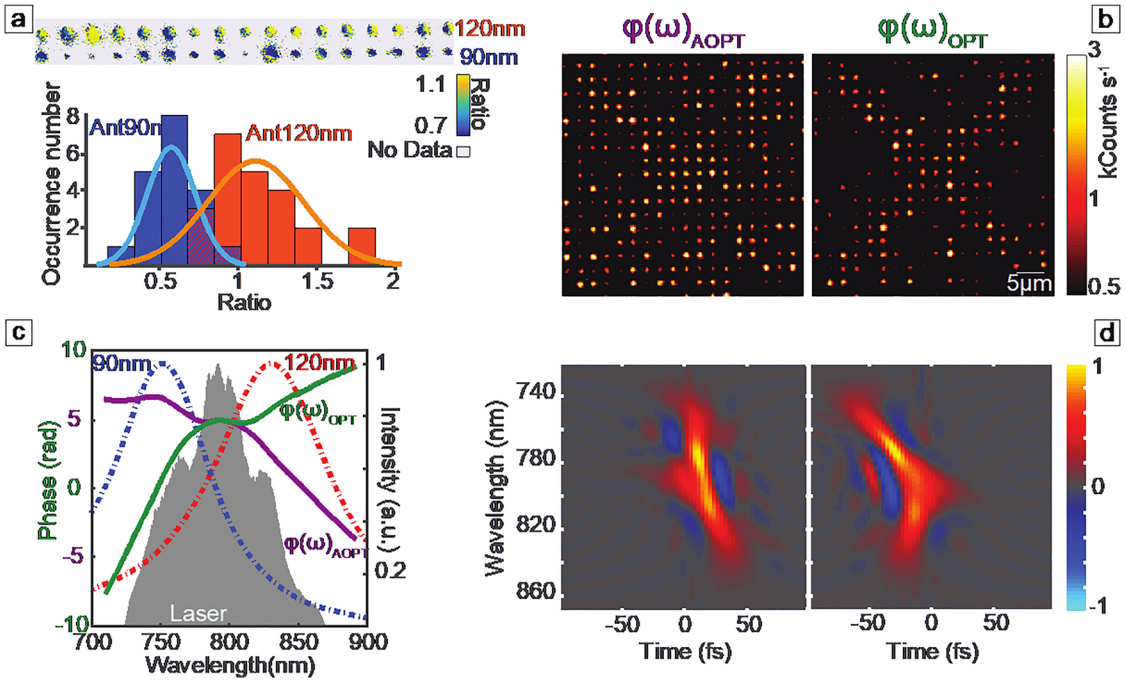

Figure 3: Coherent control of nanoantenna arrays.
(a) The upper image is the ratio between the TPPL images of an array of nanoantenna pairs obtained with $\varphi(\omega)_{OPT}$ and $\varphi(\omega)_{AOPT}$, respectively. Nanoantennas of 120 nm are brighter when using $\varphi(\omega)_{OPT}$, whereas the 90 nm ones are brighter when excited with $\varphi(\omega)_{AOPT}$. The histogram on the bottom quantitatively analyses the ratio of all the 90 nm antennas and 120 nm nanoantennas with the two different phases. The cyan and orange curves superimposed on the histogram are fits to the data assuming a normal distribution. Note that, in the histogram, a full array of nanoantennas is considered for the statistics (23 pairs), whereas in the upper image, a zoom on 17 pairs of nanoantennas is shown. We also note that for some of the 90 nm antennas, the TPPL intensity emitted with $\varphi(\omega)_{OPT}$ is so low that it is not taken into account in the histogram graph. (b) Two-photon–induced photoluminescence images of an array of mixed 120 and 90 nm antennas using $\varphi(\omega)_{AOPT}$ or $\varphi(\omega)_{OPT}$. The encoded message clearly appears when using $\varphi(\omega)_{OPT}$ and is erased by $\varphi(\omega)_{AOPT}$. (c) Laser spectrum (shaded region), $\varphi(\omega)_{OPT}$ (green curve) and $\varphi(\omega)_{AOPT}$ (violet curve) as measured with the multiphoton intrapulse interference phase scan (see Methods). The red and blue dashed curves are the resonance response of the 90 nm and the 120 nm nanoantennas as obtained by Finite-Difference Time-Domain (FDTD) simulations. (d) Time–frequency Wigner representation of the pulses corresponding to the optimization (right) and antioptimization (left) case. TPPL, two-photon–induced photoluminescence.

procedure as for Figure 2f) of one array of paired 90 and 120 nm nanoantennas, obtained under excitation with $\varphi(\omega)_{OPT}$ and $\varphi(\omega)_{AOPT}$. From this image, one can see that changing from $\varphi(\omega)_{OPT}$ to $\varphi(\omega)_{AOPT}$ produced the same overall effect in most of the 90–120 nm nanoantenna pairs. Statistical analysis is given in the histogram of Figure 3a, which helps visualizing this trend. The distribution of the ratios is clearly shifted, as confirmed by fits to the data presented in the histogram assuming a normal distribution function. The width of the distributions is caused by the intrinsic variability of fabrication, which is always present for e-beam nanofabricated antennas. It must also be noted that a higher level of control could be obtained for the 90 nm nanoantennas. By changing the spectral phase from $\varphi(\omega)_{AOPT}$ to $\varphi(\omega)_{OPT}$, the TPPL from the 120 nm nanoantennas increased on average by ~1.12, whereas that from 90 nm nanoantennas decreased by ~1.76, with a total contrast of ~2. This difference could be due to distinct coherence time for the two antenna species, as explained below.

Now, we can use this coherent selectivity in nonlinear microscopy, as shown for ensembles of molecules and quantum dots [53–56], and extend the control to the field of nanoplasmonics. Figure 3b demonstrates this concept at the level of individual nanoantennas. We fabricated an array of mixed 120 and 90 nm nanoantennas. The 120 nm nanoantennas were arranged such to form an encoded message, in this case the letter 'X', on a background of 90 nm ones. We acquired two different two-dimensional TPPL images of such array using $\varphi(\omega)_{OPT}$ and $\varphi(\omega)_{AOPT}$, respectively. As Figure 3b demonstrates, by using pure coherent control, we could deterministically reveal or completely hide the encoded message. In this case, complete switch of the TPPL maximum from 120 to 90 nm nanoantennas did not occur (as in the case of Figure 2d and f) as the 120 nm ones always emitted more TPPL. Still, clear

contrast between the two images is visible, confirming that coherent control can extract sensitive microscopic information about different resonant species.

We are now in the position to give a solid interpretation to the coherent control experiment, as illustrated in the bottom panel of Figure 3. In Figure 3c, we plot the excitation laser spectrum, together with the spectral phases $\varphi(\omega)_{\mathrm{OPT}}$ and $\varphi(\omega)_{\mathrm{AOPT}}$ obtained after the optimization. The blue and red dashed curves correspond to the LSPR profiles for the 90 and 120 nm nanoantennas, respectively, as obtained from Finite-Difference Time-Domain (FDTD) simulations (see Methods). As anticipated above, the LSPR corresponding to the 90 nm antennas is resonant on the blue side and that of the 120 nm one on the red side of the laser spectrum. These curves represent the intermediate states in the TPE process, namely the terms $A(\omega)$ in Eq. (1). From this plot, it is apparent that the two spectral phases $\varphi(\omega)_{\mathrm{OPT}}$ and $\varphi(\omega)_{\mathrm{AOPT}}$ have symmetric behaviours with respect to the positions of the LSPRs.

As both the time and the frequency information is relevant for the interpretation of the current experiment, in Figure 3d, we report the time–frequency representation (details in the study by Paye [57]) for the two electric fields corresponding to the optimization (right) and antioptimization (left) case, respectively. In the spectral domain (vertical axis of the plots), one can see that in the optimization case, the red part of the laser spectrum is only slightly distorted (it is almost a straight line at time zero), whereas the blue part of it is chirped. A flat spectral phase drives the 120 nm antenna, whereas a dispersed spectral phase drives the 90 nm antenna. The opposite situation is found for the antioptimization case, and the respective time–frequency Wigner representations are almost inverted along their time development. The effect of coherent control is therefore to distort the pulse in the spectral region of the unwanted LSPR and make TPE through the desired plasmon resonance more favourable. This is consistent with our findings that $\varphi(\omega)_{\mathrm{OPT}}$ optimizes the TPPL ratio between 120 and 90 nm antennas and vice versa. However, as explained above, the phase control is only effective for short enough pulses (within the coherent regime of Figure 1b), whereas for longer pulses, the spectral phase has no effect. Indeed, the pulses represented in Figure 3d are still very short, with a total duration of less than 50 fs and therefore can interact coherently with the nanoantennas. Note that our algorithm optimizes on the differences between the nanoantennas, without any assumption on coherent or incoherent regimes. The algorithm, in the configuration used [40], has the capability to stretch the pulse beyond 200 fs and could have ended up in pulses longer than the coherence time. Instead, the algorithm choses to exploit the phase and chirp the pulse in a selected spectral regime. This again confirms the validity of the three-level model discussed above.

As a final confirmation that the interpretation given here is correct, we calculated the contrast in the TPE probability in the two nanoantennas using Eq. (2), which is approximately valid in the very short pulse regime. To do so, we considered the resonant curves of Figure 3c as the excitation lineshapes (the $A(\omega)$ terms) of the nanoantennas and calculated the laser electric field based on the measurements of the laser spectrum and the spectral phases $\varphi(\omega)_{\mathrm{OPT}}$ and $\varphi(\omega)_{\mathrm{AOPT}}$. The calculated TPE probabilities are in good agreement with the experiment, yielding a contrast of ~2.0 for the 90 nm nanoantenna and of ~1.3 for the 120 nm one, with a total contrast of ~2.6. The spectral width of the LSPR is wider for the 120 nm nanoantenna, i.e. the longer antenna is more lossy and the coherence time T_2 is shorter. The algorithm changes the phase and therefore the time duration of the laser pulse and reaches first the incoherent regime of the 120 nm before the 90 nm nanoantenna. As a result, the algorithm has a larger time–frequency parameter space to distort the pulse in the case of the shorter 90 nm nanoantenna, as in fact shown by the time–frequency representations in Figure 3d, and higher contrast is obtainable for the 90 nm nanoantennas.

4 Conclusions

In this work, we have presented a detailed and comprehensive study of the TPE process and its dependence on the phase of an ultrashort laser pulse in gold nanoantennas. We have shown that two relevant timescales govern the dynamics of the two-step excitation process: the dephasing time of the localized surface plasmons and the lifetime of the intermediate state involved. For very short pulses with duration shorter than or comparable to the plasmon dephasing time, the TPE in resonant gold nanoantennas is sensitive to the spectral phase of the laser pulse and coherent control becomes possible. For longer pulses (longer than 100 fs), no phase control of the gold nanoantennas is possible. The less lossy high-index semiconductor antennas might be interesting for control at longer timescales [58].

We have subsequently demonstrated pure coherent phase control by using a closed-loop optimization strategy that actively manipulates the coherence of surface plasmons to selectively excite two different nanoantennas solely by shaping the laser spectral phase. This is a conclusive demonstration of highly sensitive closed-loop coherent control on the nanoscale.

5 Methods

The laser source used in the experiment was a broadband titanium sapphire laser (Octavius 85 M, Menlo System, Menlo Systems GmbH, Am Klopferspitz 19a, D-82152 Martinsried, Germany) with a spectrum centred at 800 nm and with bandwidth of ~150 nm. The pulse shaper was arranged in a 4-f configuration, and the active element was a spatial light modulator composed by two 640-pixel liquid crystal masks. The pulse shaper was used exclusively for phase shaping, and no amplitude shaping was performed.

In the pulse duration dependence experiment, the laser beam was sent to a confocal microscope and focused on the sample from the bottom by a 1.4 numerical aperture (NA) objective. The sample was mounted on a nanometre precision piezoelectric scanner for two-dimensional imaging. The nonlinear signals generated at the sample were collected through the same objective, spectrally filtered to cut the reflected laser light and sent to the photodetector: a Si APD in counting mode. The pulse shaper was used to change the pulse duration by applying different amounts of linear chirp.

The $BaTiO_3$ nanoparticles were purchased from Sigma-Aldrich: Sigma-Aldrich, Inc., nanopowder (cubic crystalline phase), <100 nm particle size, ≥99% trace metals basis, dispersed in ethanol, and deposited onto a microscope coverslip, following a previously developed procedure [49].

In the closed-loop coherent control experiment, the laser was focused from the top of the sample by a 0.15 NA objective on the sample containing the gold nanoantennas. The lateral size of the excitation spot at the sample position was about 8 μm and, together with the arrangement of the nanoantennas in the sample, was chosen such that two different nanoantennas could be excited at the same time. The excitation polarization was kept circular in the experiment. The TPPL was collected in transmission through the 1.4 NA objective and sent to two different APDs after being separated by a beam splitter. The combination of the 1.4 NA objective, the system of lenses that focused the light on the APDs and the physical size of the active area of the APDs was such that the APDs receive light form a much smaller area than the excitation spot, being roughly of 1 μm. This allowed us to spatially distinguish between one and the other nanoantenna and to change the actual detection area by spatially displacing the APDs. By slightly moving the two APDs in different directions, we could align them on the TPPL emitted by the two different nanoantennas.

The nanoantennas studied were gold nanorods of length varying between 90 and 190 nm, fabricated using electron beam lithography on a glass coverslip coated with a 10 nm-thin layer of indium tin oxide (ITO). The width and height of the nanoantennas were both fixed at 50 nm, and they were fabricated to be resonant with different portions of the laser spectrum. In order to study two nanoantennas characterized by different LSPRs at the same time, they were arranged in pairs of different lengths separated by 2 μm.

The spectral phases shown in Figure 3c were measured using the MIIPS described in the studies by Xu et al. [50] and Galvan-Sosa et al. [52] combined with SH nanoparticles, following a method we previously developed [49].

The extinction spectra of the nanoantennas were calculated using FDTD Solutions (Lumerical Inc.): www.Lumerical.com, Lumerical Inc., 1700–1095 West Pender Street, Vancouver, BCV6E 2M6, Canada. The nanoantennas themselves were 130 × 40 × 40 and 100 × 40 × 40 nm^3, with the top corners rounded (radius = 10 nm) to approximate the fabricated nanoantennas. The nanoantenna lied on a 10 nm layer of ITO, which was itself on silicon dioxide. The permittivity of Au was taken using a fit of Palik's data, and the ITO data were taken from in-house measurements and also fitted, in both cases using their multicoefficient model of the experimental data. The mesh size was 2 nm and encompassed the entire nanoantenna. The source was a total field scattered field (TFSF) plane wave at normal incidence to the glass surface, injected from within the air side. To measure the absorbed and scattered powers, plane monitors were arranged to form two boxes around the nanoantenna, one inside and one outside of the TFSF source volume, and each monitor recorded the power transmitted through its planar surface. Given the nature of the TFSF source (i.e. it subtracts the source fields at the edge of its defined volume), the power box outside was used to calculate the scattering spectrum and the one inside to calculate the absorption. An identical simulation without nanoantenna was also realized to calculate the ITO absorption, which is then subtracted from each nanoantenna's absorption spectrum.

Author contribution: All the authors have accepted responsibility for the entire content of this submitted manuscript and approved submission.

Research funding: This research was funded by the European Commission (ERC Adv. Grant 670949-LightNet); Spanish Severo Ochoa Programme for Centres of Excellence in R&D (SEV-2015-0522); Plan National Projects MICINN FIS2012-35527, MINECO FIS2015-69258-P and MCIU PGC2018-096875-B-I00 and cofunded by the Fondo Europeo de Desarrollo Regional (FEDER); the Catalan AGAUR (2014 SGR01540 and 2017 SGR1369); Fundació Privada Cellex; Fundació Privada Mir-Puig and Generalitat de Catalunya through the Centres de Recerca de Catalunya (CERCA) program. PMdR acknowledges financial support from the Spanish Government MINECO-FPI grant and European Science Foundation under the PLASMON-BIONANOSENSE Exchange Grant program. MGS acknowledges financial support from grants MICINN TEC2011-22422 and MINECO TEC2014-52642-C2-1-R.

Conflict of interest statement: The authors declare no conflicts of interest regarding this article.

References

[1] D. J. Tannor, R. Kosloff, and S. A. Rice, "Coherent pulse sequence induced control of selectivity of reactions: exact quantum mechanical calculations," *J. Chem. Phys.*, vol. 85, pp. 5805–5820, 1986.

[2] M. Shapiro and P. Brumer, *Quantum Control of Molecular Processes*, Wiley-VCH Verlag GmbH & Co. KGaA, 2011, https://doi.org/10.1002/9783527639700.

[3] M. Dantus and V. V. Lozovoy, "Experimental coherent laser control of physicochemical processes," *Chem. Rev.*, vol. 104, pp. 1813–1859, 2004.

[4] P. Nuernberger, G. Vogt, T. Brixner, and G. Gerber, "Femtosecond quantum control of molecular dynamics in the condensed phase," *Phys. Chem. Chem. Phys.*, vol. 9, p. 2470, 2007.

[5] C. Brif, R. Chakrabarti, and H. Rabitz, "Control of quantum phenomena: past, present and future," *New J. Phys.*, vol. 12, 2010. https://doi.org/10.1088/1367-2630/12/7/075008.
[6] Y. Silberberg, "Quantum coherent control for nonlinear spectroscopy and microscopy," *Annu. Rev. Phys. Chem.*, vol. 60, pp. 277–292, 2009.
[7] L. Novotny and N. F. van Hulst, "Antennas for light," *Nat. Photon.*, vol. 5, pp. 83–90, 2011.
[8] A. G. Curto, G. Volpe, T. H. Taminiau, et al., "Unidirectional emission of a quantum dot coupled to a nanoantenna," *Science*, vol. 329, pp. 930–933, 2010.
[9] I. M. Hancu, A. G. Curto, M. Castro-López, M. Kuttge, and N. F. van Hulst, "Multipolar interference for directed light emission," *Nano Lett.*, vol. 14, pp. 166–171, 2014.
[10] D. Vercruysse, X. Zheng, Y. Sonnefraud, et al., "Directional fluorescence emission by individual V-antennas explained by mode expansion," *ACS Nano*, vol. 8, pp. 8232–8241, 2014.
[11] G. Zengin, M. Wersäll, S. Nilsson, et al., "Realizing strong light-matter interactions between single-nanoparticle plasmons and molecular excitons at ambient conditions," *Phys. Rev. Lett.*, vol. 114, p. 157401, 2015.
[12] A. Kinkhabwala, Z. Yu, S. Fan, et al., "Large single-molecule fluorescence enhancements produced by a bowtie nanoantenna," *Nat. Photon.*, vol. 3, pp. 654–657, 2009.
[13] E. Wientjes, J. Renger, A. G. Curto, R. Cogdell, and N. F. van Hulst, "Strong antenna-enhanced fluorescence of a single light-harvesting complex shows photon antibunching," *Nat. Commun.*, vol. 5, pp. 1516–1519, 2014.
[14] M. Kauranen and A. V. Zayats, "Nonlinear plasmonics," *Nat. Publ. Gr.*, vol. 6, pp. 737–748, 2012.
[15] S. S. Aćimović, M. A. Ortega, V. Sanz, et al., "LSPR chip for parallel, rapid, and sensitive detection of cancer markers in serum," *Nano Lett.*, vol. 14, pp. 2636–2641, 2014.
[16] P. Zijlstra, P. M. R. Paulo, and M. Orrit, "Optical detection of single non-absorbing molecules using the surface plasmon resonance of a gold nanorod," *Nat. Nanotechnol.*, vol. 7, pp. 379–382, 2012.
[17] P. Ghenuche, S. Cherukulappurath, T. H. Taminiau, N. F. van Hulst, and R. Quidant, "Spectroscopic mode mapping of resonant plasmon nanoantennas," *Phys. Rev. Lett.*, vol. 101, p. 116805, 2008.
[18] P. Biagioni, M. Celebrano, M. Savoini, et al., "Dependence of the two-photon photoluminescence yield of gold nanostructures on the laser pulse duration," *Phys. Rev. B Condens. Matter*, vol. 80, pp. 1–5, 2009.
[19] P. Biagioni, M. H. Lee, N. J. Halas, et al., "Dynamics of four-photon photoluminescence in gold nanoantennas," *Nano Lett.*, vol. 12, pp. 2941–2947, 2012.
[20] A.M. Gobin, M. H. Lee, N. J. Halas, et al., "Near-infrared resonant nanoshells for combined optical imaging and photothermal cancer therapy," *Nano Lett.*, vol. 7, pp. 1929–1934, 2007.
[21] N. J. Durr, T. Larson, D. K. Smith, et al., "Two-photon luminescence imaging of cancer cells using molecularly targeted gold nanorods," *Nano Lett.*, vol. 7, pp. 941–945, 2007.
[22] N. Gao, Y. Chen, L. Li, et al., "Shape-dependent two-photon photoluminescence of single gold nanoparticles," *J. Phys. Chem. C*, vol. 118, pp. 13904–13911, 2014.
[23] M. I. Stockman, S. V. Faleev, and D. J. Bergman, "Coherent control of femtosecond energy localization in nanosystems," *Phys. Rev. Lett.*, vol. 88, pp. 67402/1–67402/4, 2002.
[24] M. I. Stockman, "Ultrafast nanoplasmonics under coherent control," *New J. Phys.*, vol. 10, 2008. https://doi.org/10.1088/1367-2630/10/2/025031.
[25] M. Aeschlimann, M. Bauer, D. Bayer, et al., "Spatiotemporal control of nanooptical excitations," *Proc. Natl. Acad. Sci. USA*, vol. 107, pp. 5329–5333, 2010.
[26] M. Aeschlimann, M. Bauer, D. Bayer, et al., "Adaptive subwavelength control of nano-optical fields," *Nature*, vol. 446, pp. 301–304, 2007.
[27] A. Kubo, K. Onda, H. Petek, et al., "Femtosecond imaging of surface plasmon femtosecond imaging of surface plasmon dynamics in a nanostructured silver film," *Nano*, vol. 5, pp. 1123–1127, 2005.
[28] Q. Sun, K. Ueno, H. Yu, et al., "Direct imaging of the near field and dynamics of surface plasmon resonance on gold nanostructures using photoemission electron microscopy," *Light Sci. Appl.*, vol. 74, p. e118, 2013.
[29] T. Hanke, J. Cesar, V. Knittel, et al., "Tailoring spatiotemporal light confinement in single plasmonic nanoantennas," *Nano Lett.*, vol. 12, pp. 992–996, 2012.
[30] R. Mittal, R. Glenn, I. Saytashev, V. V. Lozovoy, and M. Dantus, "Femtosecond nanoplasmonic dephasing of individual silver nanoparticles and small clusters," *J. Phys. Chem. Lett.*, vol. 6, pp. 1638–1644, 2015.
[31] E. Mårsell, A. Losquin, R. Svärd, et al., "Nanoscale imaging of local few-femtosecond near-field dynamics within a single plasmonic nanoantenna," *Nano Lett.*, vol. 15, pp. 6601–6608, 2015.
[32] Y. Nishiyama, K. Imaeda, K. Imura, and H. Okamoto, "Plasmon Dephasing in Single Gold Nanorods Observed by Ultrafast Time-Resolved Near-Field Optical Microscopy," *J. Phys. Chem. C*, vol. 119, pp. 16215–16222, 2015.
[33] Y. Nishiyama, K. Imura, and H. Okamoto, "Observation of plasmon wave packet motions via femtosecond time-resolved near-field imaging techniques," *Nano Lett.*, vol. 15, pp. 7657–7665, 2015.
[34] J. M. Gunn, S. H. High, V. V. Lozovoy, and M. Dantus, "Measurement and control of ultrashort optical pulse propagation in metal nanoparticle-covered dielectric surfaces," *J. Phys. Chem. C*, vol. 114, pp. 12375–12381, 2010.
[35] J. M. Gunn, M. Ewald, and M. Dantus, "Polarization and phase control of remote surface-plasmon-mediated two-photon-induced emission and waveguiding," *Nano Lett.*, vol. 6, pp. 2804–2809, 2006.
[36] K. Imura, T. Nagahara, and H. Okamoto, "Near-field two-photon-induced photoluminescence from single gold nanorods and imaging of plasmon modes," *J. Phys. Chem. B*, vol. 109, pp. 13214–13220, 2005.
[37] X.-F. Jiang, Y. Pan, C. Jiang, et al., "Excitation nature of two-photon photoluminescence of gold nanorods and coupled gold nanoparticles studied by two-pulse emission modulation spectroscopy," *J. Phys. Chem. Lett.*, vol. 4, pp. 1634–1638, 2013.
[38] K. Imaeda and K. Imura, "Optical control of plasmonic fields by phase-modulated pulse excitations," *Opt. Express*, vol. 21, p. 27481, 2013.
[39] D. Brinks, M. Castro-Lopez, R. Hildner, and N. F. van Hulst, "Plasmonic antennas as design elements for coherent ultrafast nanophotonics," *Proc. Natl. Acad. Sci. USA*, vol. 110, pp. 18386–18390, 2013.

[40] N. Accanto, P. M. de Roque, M. Galvan-Sosa, S. Christodoulou, I. Moreels and N. F. van Hulst, "Rapid and robust control of single quantum dots," *Light Sci. Appl.*, vol. 6, p. e16239, 2016.
[41] V. V. Lozovoy, I. Pastirk, K. A. Walowicz, and M. Dantus, "Multiphoton intrapulse interference. II. Control of two- and three-photon laser induced fluorescence with shaped pulses," *J. Chem. Phys.*, vol. 118, pp. 3187–3196, 2003.
[42] N. Del Fatti, C. Voisin, M. Achermann, et al., "Nonequilibrium electron dynamics in noble metals," *Phys. Rev. B*, vol. 61, pp. 16956–16966, 2000.
[43] C.-K. Sun, F. Vallée, L. H. Acioli, E. P. Ippen, and J. G. Fujimoto, "Femtosecond-tunable measurement of electron thermalization in gold," *Phys. Rev. B*, vol. 50, pp. 15337–15348, 1994.
[44] A. Block, M. Liebel, R. Yu, F.J. García de Abajo, Y. Sivan, and N.F. van Hulst, "Tracking ultrafast hot-electron diffusion in space and time by ultrafast thermo-modulation microscopy," *Sci. Adv.*, vol. 5, p. eaav8965, 2019.
[45] A. Anderson, K. S. Deryckx, X. G. Xu, G. Steinmeyer, and M. B. Raschke, "Few-plasmon dephasing of a single metallic nanostructure from optical response function reconstruction by interferometric frequency resolved optical gating," *Nano Lett.*, vol. 10, pp. 2519–2524, 2010.
[46] N. Dudovich, B. Dayan, S. M. Gallagher Faeder, and Y. Silberberg, "Transform-limited pulses are not optimal for resonant multiphoton transitions," *Phys. Rev. Lett.*, vol. 86, pp. 47–50, 2001.
[47] S. Zhang, C. Lu, T. Jia, J. Qiu, and Z. Sun, "Coherent phase control of resonance-mediated two-photon absorption in r femtosecond are-earth ions," *Appl. Phys. Lett.*, vol. 103, pp. 1–5, 2013.
[48] N. Accanto, L. Piatkowski, J. Renger, and N. F. van Hulst, "Capturing the optical phase response of nanoantennas by coherent second-harmonic microscopy," *Nano Lett.*, vol. 14, pp. 4078–4082, 2014.
[49] Y. Coello, V. V. Lozovoy, T. C. Gunaratne, et al., "Interference without an interferometer: a different approach to measuring, compressing, and shaping ultrashort laser pulses," *J. Opt. Soc. Am. B*, vol. 25, p. A140, 2008.
[50] B. Xu, J. M. Gunn, J. M. Dela Cruz, V. V. Lozovoy, and M. Dantus, "Quantitative investigation of the multiphoton intrapulse interference phase scan method for simultaneous phase measurement and compensation of femtosecond laser pulses," *J. Opt. Soc. Am. B*, vol. 23, p. 750, 2006.
[51] V. Remesh, M. Stührenberg, L. Saemisch, N. Accanto, and N.F. van Hulst, "Phase control of plasmon enhanced two-photon photoluminescence in resonant gold nanoantennas," *Appl. Phys. Lett.*, vol. 113, p. 211101, 2018.
[52] M. Galvan-Sosa, J. Portilla, J. Hernandez-Rueda, et al., "Optimization of ultra-fast interactions using laser pulse temporal shaping controlled by a deterministic algorithm," *Appl. Phys. Mater. Sci. Process*, vol. 114, pp. 477–484, 2014.
[53] T. Brixner, N. H. Damrauer, P. Niklaus, and G. Gerber, "Photoselective adaptive femtosecond quantum control in the liquid phase," *Nature*, vol. 414, pp. 57–60, 2001.
[54] M. Ruge, R. Wilcken, M. Wollenhaupt, A. Horn, and T. Baumert, "Coherent control of colloidal semiconductor nanocrystals," *J. Phys. Chem. C*, vol. 117, pp. 11780–11790, 2013.
[55] J. P. Ogilvie, D. Débarre, X. Solinas, et al., "Use of coherent control for selective two-photon fluorescence microscopy in live organisms," *Opt. Express*, vol. 14, pp. 759–766, 2006.
[56] I. Pastirk, J. Dela Cruz, K. Walowicz, V. Lozovoy, and M. Dantus, "Selective two-photon microscopy with shaped femtosecond pulses," *Opt. Express*, vol. 11, pp. 1695–1701, 2003.
[57] J. Paye, "The chronocyclic representation of ultrashort light pulses," *IEEE J. Quant. Electron.*, vol. 28, pp. 2262–2273, 1992.
[58] V. Remesh, G. Grinblat, Y. Li, S. A. Maier, and N. F. van Hulst, "Coherent multiphoton control of gallium phosphide nanodisk resonances," *ACS Photon.*, vol. 6, pp. 2487–2491, 2019.